A Novel, High Fidelity 6-DoF Simulation Model for Tethered Load Dynamics

Daniel T. Prosser* dtprosser@gatech.edu
Marilyn J. Smith† marilyn.smith@ae.gatech.edu
School of Aerospace Engineering
Georgia Institute of Technology
Atlanta, Georgia 30332

ABSTRACT

A novel, physics-based reduced-order model for the simulation of tethered loads and other dynamic bluff bodies in six-degree-of-freedom motion has been developed. The reduced-order aerodynamic model is founded on physical insights and supporting data from quasi-steady computational fluid dynamics simulations, experiments, or flight tests. The reduced-order model incorporates quasi-steady aerodynamics, unsteady vortex shedding phenomena, and unsteady aerodynamic effects of body motion. The reduced-order model accurately reproduces dynamics predicted by computational fluid dynamics simulations, while computational cost is reduced by more than five orders of magnitude. The methodology can readily be applied or extended to any bluff body geometry beyond those demonstrated in this work. Guidance is provided for the relatively minor modifications to include rotor downwash, atmospheric turbulence, and wind tunnel walls.

NOTATION

b	Reference length, m
C_ζ	Aerodynamic coefficient, $C_\zeta = \frac{2\zeta}{\rho U_\infty^2 S_{ref}}$ for ζ a force or $C_\zeta = \frac{2\zeta}{\rho U_\infty^2 S_{ref} b}$ for ζ a moment
$H_n^{(m)}$	Hankel function of order m and kind n
$\boldsymbol{I_{xx}}$, $\boldsymbol{I_{yy}}$, $\boldsymbol{I_{zz}}$	Moments of inertia, kg-m^2
k	Reduced frequency, $k = \frac{\omega b}{U_\infty}$
s	Laplace variable
S_{ref}	Reference area, m^2
t	Time variable, sec
$\boldsymbol{V}_{cg}$	Tethered load velocity vector, m/sec
$\boldsymbol{U}_\infty$	Reference velocity vector, m/sec
$\boldsymbol{W}$	Relative wind vector, m/sec
α, β	Angle of attack and yaw, deg.
ε, η, ω_n, ω_{nqs}	Unsteady aerodynamic model parameters
ω	Frequency of body motion, rad/sec
ω_s	Frequency of vortex shedding, rad/sec
ζ	Aerodynamic force or moment
$\overline{()}$	Mean-flow quantity
$()'$	Fluctuating quantity

Subscripts and superscripts

^{qs}	Quasi-steady coefficient
$_0$	Reference value of a coefficient

INTRODUCTION

The coupled aerodynamic-dynamic behavior of bluff bodies is important in many engineering fields. These interactions are of particular interest to the rotorcraft community, as it is common for helicopters to carry large payloads slung underneath the vehicle by tethers. In military operations, this approach is often taken to deliver supplies or equipment to operational theaters. In civilian applications, tethered loads are common in performing rescue operations, in carrying equipment to remote or disaster locations, and in aerial firefighting to increase the payload volume of the helicopter. In air drops, the coupled aerodynamics and dynamics of the payload determine where and how it will land. Aerodynamic-dynamic interactions of bluff bodies are also key in the structural and wind engineering fields, as tall buildings, towers, suspension bridges, and power lines are subject to these phenomena (Refs. 1–5). Therefore, understanding and predicting these complex interactions is critical during design and mission planning for a broad range of applications.

In current helicopter tethered load operations, the flight envelope may be significantly reduced, in part because of the added drag of the load, but more significantly because of instabilities arising from dynamic motion of the load (Refs. 6,7). Instabilities result from the excitation of large-magnitude unsteady aerodynamic forces and moments acting on the bluff

*Ph.D. Candidate and Graduate Research Assistant, AHS student member

†Professor, AHS member

Presented at the AHS 70th Annual Forum, Montréal, Québec, Canada, May 20–22, 2014.

body. These dynamic effects can be particularly severe, culminating in large excursions of the load, excessive vertical motions of the helicopter and load, tether instabilities, or a combination of all three (Refs. 6, 8). As an example of flight envelope reduction, the power-limited forward speed of the UH-60 helicopter with the CONEX cargo container is above 100 knots, but the stability-limited forward speed is just 60 knots (Ref. 7).

Over the past decade, understanding and prediction of the dynamics of tethered loads in flight have become priorities, in part due to the problems encountered during Hurricane Katrina rescue efforts. A wide variety of techniques have been evaluated, including wind tunnel testing, flight testing, computational fluid dynamics (CFD) simulation, and reduced-order modeling. Raz et al. (Ref. 9) and Cicolani et al. (Ref. 10) applied wind tunnel testing to focus on passive stabilization of tethered load dynamics, demonstrating that significantly higher safe flight speeds were possible with the addition of aerodynamic fins. Raz et al. (Ref. 11) employed flight testing to investigate coupled helicopter-load dynamics and pilot-induced oscillations in tethered load operations. Comparisons with his prior efforts led to the conclusion that results of careful wind tunnel tests of scaled load geometries may provide good correlation with flight test data.

Greenwell (Ref. 6) developed empirical relations for the quasi-steady forces and moments acting on two-dimensional and three-dimensional rectangular boxes. These relations are designed to reproduce the observed variations of separation and reattachment with incidence angles and changes in aspect ratio. As such, they are invaluable in completing quasi-steady data sets of configurations lacking extensive test data. Prosser and Smith (Ref. 12) also utilized experimental and computational data available in the literature to demonstrate that, for two-dimensional and three-dimensional rectangular box geometries, there exists a region where the transverse force remains approximately constant with changes in incidence angle. They mathematically demonstrated that this region collapses onto a single empirical curve fit as a function of aspect ratio, reducing the need for extensive testing or simulation.

Other researchers have studied the behavior of tethered loads using simulation. For example, Cicolani and Kanning (Ref. 13) developed equations of motion for simulation of rotorcraft carrying suspended loads, but they did not consider the problem of modeling the aerodynamic forcing terms. Cicolani and da Silva (Ref. 14) investigated the aerodynamic forcing problem for the CONEX container. Their aerodynamic model was derived from system identification of the aerodynamics in the frequency domain, which was then transferred to the time domain for simulation. Their initial formulation, developed from unsteady CFD simulations, was two-dimensional and linear, considering only yaw motion. Further development of this model was presented by Cone (Ref. 15). In this case, the quasi-steady yaw moment was interpolated from tabulated wind tunnel data as a function of the aerodynamic angles. Frequency-domain decomposition of flight test data was then performed to establish transfer functions between the quasi-steady and unsteady yaw moment at a number of different flight speeds. Favorable correlation between the model and flight test data was produced at some flight speeds, but application of this approach was somewhat restricted as it requires a new transfer function for each flight condition and configuration, preventing rapid extensibility to different flight speeds, aspect ratios, Mach numbers, and Reynolds numbers.

The effect of wind tunnel walls in tethered-load dynamics was examined by Sharma et al. (Ref. 16) via a two-dimensional single point potential flow source-image method. This study implied that wind tunnel walls can influence the dynamics of tethered loads, but it did not consider unsteady aerodynamic effects or six-degree-of-freedom (6-DoF) dynamics. In a first-principles simulation approach, Prosser and Smith (Ref. 17) applied three-dimensional unsteady Reynolds-averaged Navier Stokes (URANS) computations with large-eddy-simulation (LES) turbulence closure in the wake, coupled with a 6-DoF rigid body motion solver to simulate the dynamics of a tethered load. Though this very high-fidelity capability is promising in terms of prediction accuracy and generalizability, the cost is too high for rapid assessment of stability and sensitivity of new configurations and operational conditions.

Prior art indicates that reduced-order aerodynamic models may be very accurate when they are drawn from high-fidelity data from experiments, flight testing, or computations, and when they sufficiently address the important physics of the problem. The most well-known of these models are the finite-state and unified unsteady aerodynamics theories of Peters et al. (Refs. 18–20). To develop these models, time-accurate Navier-Stokes-based computation is especially useful for evaluating quasi-steady aerodynamics because, compared to flight or wind tunnel testing, it is relatively inexpensive to assess the range of configurations and conditions needed to create a reduced-order model. The details of the flow field can also provide a high level of insight into the flow physics.

To date most of the reduced-order models for tethered-load aerodynamics function as "black boxes" that tune parameters to match an observed response (Refs. 15, 21); response surface and Kriging techniques are examples of this type of approach. These types of models typically do not interpolate or extrapolate accurately in conditions where data is sparse (Ref. 22). This results in reduced confidence that this approach will accurately represent new configurations, size and velocity scales, or flight regimes. In addition, dynamic models based on these techniques require significant investment in a suite of dynamic simulations or tests to bracket the potential behavior (Ref. 23), obviating the purpose of the reduced-order simulation.

A new *physics-based* reduced-order model has been developed and assessed. The model draws on quasi-steady data from time-accurate three-dimensional computations or experiments. The unsteady aerodynamic model is based on classical aerodynamic theory in the time domain, augmented by empirical corrections of the primary vortex shedding of bluff bodies from computations or experiments. This approach is

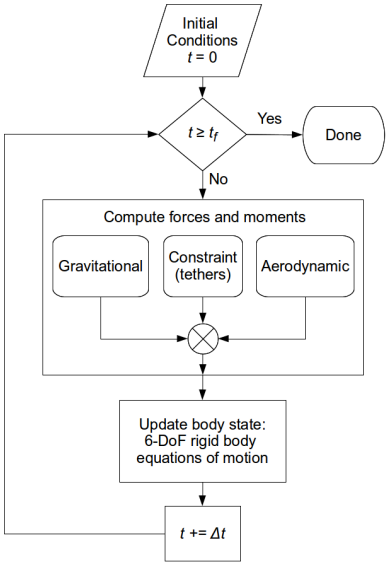

Fig. 1: Overall 6-DoF simulation model

modular and generalizable to any bluff body configuration. The physics-based aerodynamics model provides confidence in its accuracy over a broad range of conditions. The reduced-order model algorithms are presented and demonstrations validate that it accurately and rapidly predicts tethered load dynamics in comparison with much more expensive coupled URANS/6-DoF simulations.

MODEL DEVELOPMENT

The reduced-order aerodynamic model is one component of the overall dynamic simulation model which is illustrated in Fig. 1. The overall model simulates rigid bodies in 6-DoF motion subject to gravity, aerodynamic forces and moments, and constraints arising from the tether system. Orientations are formulated in terms of four quaternions, and the 6-DoF equations are solved in the body frame. Tether constraints are implemented as additional forces and moments applied to the rigid body. Each cable that comprises part of the tether system is treated as a combined linear spring and damper element whose force acts along the line between its two endpoints. Cable mass, curvature, and aerodynamics are neglected in the current model, but the implementation of the tether system in the overall model is modular, so enhancements can be easily added. Additional details on the simulation model, including the 6-DoF equations of motion and the cable forces and moments, can be found in Prosser and Smith (Ref. 17).

The remainder of the model development section deals with the aerodynamics module in the simulation model. A successful reduced-order aerodynamic model must incorporate the causal physics of the problem. In the case of bluff bodies, there are three major phenomena that contribute to the overall aerodynamic forces and moments:

1. Quasi-steady phenomena determine the mean loading at a given orientation. These effects are present in all aerodynamics problems, and for many flight dynamics applications they represent the largest contribution to the overall forces and moments.

2. Unsteady, fluctuating forces and moments arise from vortex shedding. These effects are significant in bluff body configurations as large regions of separated flow containing energetic vortical structures exist. These oscillating or Strouhal shedding processes contribute to large unsteady fluctuations in integrated aerodynamic coefficients. In contrast, in non-bluff-body configurations where attached flow dominates, the vortex shedding phenomenon can be of minor importance.

3. When body dynamics are present, additional unsteady phenomena exist even in attached flow. These unsteady effects are a consequence of the time required for the wake to establish a new equilibrium when a change in the body's orientation or velocity occurs. This creates inertial or "added mass" reaction forces and moments from the fluid (air) on the body during accelerations. These unsteady effects modify the quasi-steady mean-flow forces and moments by introducing phase lags and magnitude attenuations that impact dynamic stability.

All three of these phenomena must be included to accurately simulate the dynamic motion of a tethered load. The formulation of these phenomena into a reduced-order model is illustrated in Fig. 2. All of the parameters and quasi-steady data for the model are expressed in non-dimensional form to maximize the extensibility of the model for configurations of different sizes and flight conditions. To develop a cost-effective model of sufficient fidelity, several assumptions were applied in the derivation of this initial model:

1. Quasi-steady forces and moments are assumed to behave quasi-linearly. Nonlinearities of these quantities with changing orientation angles are measured or computed separately, with the other reference angles held constant. These permutations are superposed linearly during simulation when the angles are not at the reference values. This assumption allows nonlinear effects, including flow separation and reattachment, to be captured while retaining a simple algebraic form suitable for rapid computation.

2. The Strouhal number, $\frac{\omega_s b}{U_\infty}$, is assumed to remain constant with changes in orientation angles and upstream velocity. Therefore, the dimensional shedding frequency, ω_s, varies proportionally with the upstream velocity. This engineering assumption is reinforced by experimental data for typical bluff bodies which indicate that the Strouhal number does not change with Reynolds number in the fully-turbulent flow regime (Refs. 24, 25).

3. Unsteady aerodynamics originating from body motion are assumed to be similar to that predicted by classical unsteady aerodynamic theory (Ref. 26), despite the viscous nature of the problem and the non-planar wake.

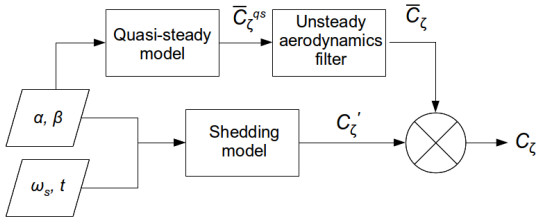

Fig. 2: Reduced-order aerodynamic model components

This assumption permits a universal treatment of these unsteady effects. Although some accuracy may be lost by the planar-wake and inviscid assumptions of the theory, recent evaluations of Theodorsen theory with viscous simulations or experiments reinforce the validity of this assumption (Ref. 27).

Quasi-Steady Model

An accurate representation of the quasi-steady aerodynamic loading is the first step in creating a high-fidelity reduced-order aerodynamic model. In this work, computational fluid dynamics (CFD) data validated for turbulent bluff body flows (Refs. 17, 28) was employed to develop the quasi-steady data set. The details of the CFD solver, grids, and conditions for computation of the quasi-steady aerodynamic coefficients for the box geometry are presented in Prosser and Smith (Ref. 17). These computations have been shown to be some of the most accurate to date in the literature, thanks in large part to a turbulence approach, known as hybrid RANS-LES, which resolves large-scale turbulence in the wake (Ref. 29), and to a feature-based unsteady overset grid adaptation capability (Ref. 30).

A "perfect" quasi-steady model would be one with data available at all possible orientations. However, measuring or computing such an extensive data set is not practical for many engineering applications. Instead, a cost-effective approach is to independently assess the sensitivity of the quasi-steady coefficients of each aerodynamic angle. This approach permits nonlinearities to be captured while maintaining a reasonable cost. The resulting form is referred here as "quasi-linear", as it is constructed by superposition of nonlinear angular variations. A representation of a generic quasi-linear aerodynamic coefficient may be written as

$$C_\zeta^{qs}(\alpha,\beta) = C_{\zeta_0}^{qs} + \alpha C_{\zeta_\alpha}^{qs}(\alpha) + \beta C_{\zeta_\beta}^{qs}(\beta). \tag{1}$$

Figure 3 illustrates how nonlinearities, resulting in large part from shear layer separation and reattachment, can be incorporated in the model without data at every possible orientation. Specifically, this figure depicts the variation of side force with yaw angle for a rectangular box representative of a CONEX container. Portions of the curve are nearly linear, but the linear trend is abruptly arrested when reattachment occurs. These nonlinearities in the quasi-steady loading significantly impact on the stability of the bluff body when it is carried in

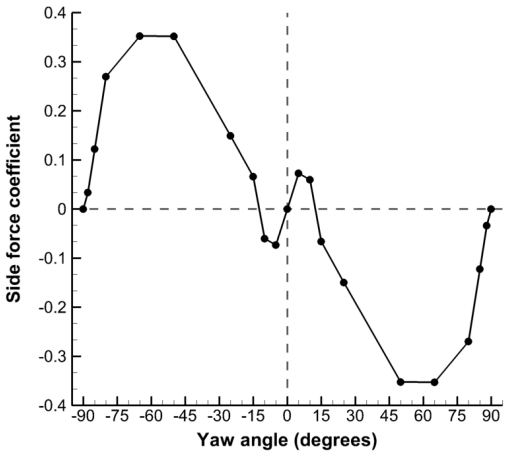

Fig. 3: Variation of side force with yaw angle, showing significant nonlinearities

a tethered configuration (Ref. 6), for instance by reducing or negating aerodynamic stiffness. The data shown in Fig. 3 can be maintained in a look-up table or a series of equations that defines the functional form of the term $C_{Y_\beta}^{qs}(\beta)$.

The aerodynamic angles (e.g., the angle of attack and yaw angle) are determined by evaluating the direction of the wind vector relative to the body axes. The wind vector is also applied as the reference when evaluating the forces and moments as coefficients. Assuming the tethered load is hanging from a fixed point in a wind tunnel or from a rotorcraft traveling at constant speed, the wind vector is

$$\boldsymbol{W} = \boldsymbol{U}_\infty - \boldsymbol{V}_{cg}. \tag{2}$$

URANS simulations were initially applied to compile the quasi-steady aerodynamic coefficient data; experimental or flight test data also be utilized, as illustrated in a later section. For sharp-edged loads (such as boxes) where separation is forced, the coefficients are relatively independent of Reynolds number, and the coefficients scale with size and flight speed. For geometries with separation from smooth surfaces (e.g. cylinders, spheres), some corrections may be needed to ensure proper scaling with Reynolds number, specifically when crossing from subcritical to supercritical values (Refs. 24,31).

Unsteady Model

When a body accelerates in a fluid due to a forcing function such as a change in wind speed or direction, the aerodynamic response is not instantaneous. As a result, the unsteady aerodynamic response lags the quasi-steady values, and its magnitude is also attenuated. These concepts form the basics of classical unsteady aerodynamic theory; see, for instance, Theodorsen's theory for simple harmonic motions and the indicial methods of Wagner and Küssner (Refs. 32–34).

Though the classical unsteady aerodynamic theories were derived for potential, attached flow, similar responses are observed in separated flows. Dynamic stall, where an airfoil,

wing, or rotor blade undergoing oscillations may briefly exceed the static stall angle, is one well-known unsteady separated flow phenomena with prominent phase lag and force attenuation (Ref. 35). When dynamic stall occurs, a vortex quickly grows and convects over the upper surface of the airfoil, resulting in large, rapidly-varying fluctuations of lift and pitching moment as the vortex influences the airfoil and near wake. Dynamic stall possesses many similarities with bluff body flows, including unsteady flow, vortex shedding, separation, and reattachment.

Significant research has been devoted in recent decades to empirical modeling of dynamic stall, in particular the unsteady effects of vortex shedding and wake dynamics on the loads. In Ref. 35, McAlister proposed a dynamic filter to model these unsteady aerodynamic effects. The model is formulated in the time domain, and it is second-order to model phase lags and response magnitude attenuation. The model is informed (updated) by experimental data, so it can be adjusted to produce an output similar to the observed response. This model has also been successfully used more recently by Ahaus and Peters in their unified unsteady aerodynamic theory (UAT) for predicting loads on single, multi-element, and deforming airfoils in stall (Refs. 19, 20). Their current efforts are devoted to additional nonlinear influences and extension to three dimensions.

An unsteady filter similar to those proposed by McAlister and Peters has been developed here for bluff body aerodynamic-dynamic interactions. The model is a second-order filter of the quasi-steady aerodynamic coefficients. For example, consider an unsteady aerodynamic coefficient C_ζ, which may represent any of the six force and moment coefficients, and its quasi-steady counterpart, C_ζ^{qs}. A filter model similar to the dynamic stall model is

$$\ddot{C}_\zeta + \eta \frac{U_\infty}{b}\dot{C}_\zeta + \omega_n^2 \frac{U_\infty^2}{b^2} C_\zeta = \omega_{nqs}^2 \frac{U_\infty^2}{b^2} C_\zeta^{qs} + \varepsilon \frac{U_\infty}{b} \dot{C}_\zeta{}^{qs}. \quad (3)$$

This second-order differential equation produces phase lags and different amplitude ratios relative to the quasi-steady prediction that are physically present due to the unsteady, developing wake and apparent mass effects. A significant benefit of this model is that the flight speed and configuration dimensions are inherent in the model, so the model parameters are non-dimensional and can be applied for a broad range of flight speeds and sizes.

Unsteady Model Parameters

Previous researchers have used similar dynamic filters in tethered load simulations to incorporate time delays in spinning motion (Refs. 14, 15, 36). However, the model parameters have been invariably tuned to match the output of a specific simulation or experiment. These parameters must then be modified for different flight conditions and tethered load configurations. As a result, much of the physical significance of these models is lost and they may not be readily extensible in predicting the stability for configurations or operating conditions that have not already been evaluated.

Rather than tuning the dynamic model parameters to the output from a limited number of simulations, classical unsteady aerodynamic theory is applied to determine the model parameters. This approach has the benefits that the unsteady model remains grounded in the physical foundation of aerodynamic theory, and the accuracy of the model can be quantified over a range of conditions. Consider the Theodorsen function, which is a transfer function in the frequency domain between unsteady and quasi-steady aerodynamics for simple harmonic motion of a thin airfoil:

$$c(k) = \frac{H_1^{(2)}(k)}{H_1^{(2)}(k) + iH_0^{(2)}(k)}. \quad (4)$$

The reduced frequency, k, can be represented in terms of complex variables as $-isb/U_\infty$ for simple harmonic motion. Eq. 3 can also be written in terms of the parameter k by first taking the Laplace transform and then substituting the relation $k = -isb/U_\infty$. Following this procedure, the dimensional quantities U_∞ and b vanish, and the transfer function becomes

$$\frac{\mathscr{C}_\zeta}{\mathscr{C}_\zeta^{qs}}(k) = \frac{ik\varepsilon + \omega_{nqs}^2}{-k^2 + ik\eta + \omega_n^2}. \quad (5)$$

The parameters can now be determined so that the best possible match between Eq. 5 and Eq. 4 is achieved. This procedure was performed with an optimization approach over two separate intervals for a wide range of reduced frequencies. The resulting values of the computed parameters are listed in Table 1.

Table 1: Dynamic model parameters approximating the Theodorsen function

	$k \leq 0.3$	$0.3 < k \leq 1$
η	2.891	31.27
ω_n	0.573	2.857
ε	1.822	16.24
ω_{nqs}	0.563	2.659

Figure 4 compares the amplitude and phase responses of the Theodorsen function with the new dynamic filter model. By specifying separate parameters for each of the two intervals, it is possible to obtain an accurate approximation of the Theodorsen function over a specified range of k. If desired, the same approach could be used to develop a higher-order dynamic filter with additional model parameters to achieve equivalent or higher accuracy over a broader range of reduced frequencies.

For most time-domain unsteady problems, there is no easily-recognizable reduced frequency, because the motion is not simple harmonic, or if the motion is simple harmonic, the reduced frequency is not known *a priori* to the application.

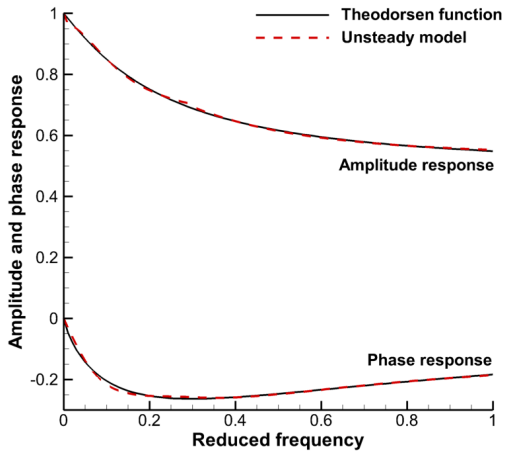

Fig. 4: Response of the frequency-domain transfer function and comparison with classical unsteady aerodynamic theory

However, for most problems the engineer is aware of the expected range of frequencies, so selection of the set of applicable model parameters from Table 1 is not problematic. In the cases presented in this work, k remains small, so the low-frequency set is selected.

Vortex Shedding Effects

In addition to the unsteady effects arising from body motion in a fluid, unsteady influences of the separated wake are present in bluff body flows. This unsteadiness is caused by vortical structures that are shed during flow separation. The result of this unsteadiness on the forces and moments is the perturbation of the quasi-steady aerodynamic coefficients. Therefore, an aerodynamic coefficient C_ζ may be represented in perturbation form:

$$C_\zeta = \overline{C}_\zeta + C'_\zeta, \tag{6}$$

where the mean-flow components are calculated as described in the previous sections. In two-dimensional laminar flows, the fluctuating terms are quite regular in nature, but in three-dimensional turbulent flows, they are much more chaotic. In order to completely represent the contributions of these fluctuating terms in turbulent flows, it is necessary to account for all the large energy-containing turbulent scales. Therefore, the fluctuating terms may be represented as

$$C'_\zeta(\alpha,\beta,t) = \sum_{i=1}^{N} C'_{\zeta,i}(\alpha,\beta)\phi(\omega_{s,i},t), \tag{7}$$

where ϕ is a function giving the time dependence of the fluctuation and N is the number of vortex shedding harmonics included. A simple representation would be $\phi(\omega_{s,i},t) = \sin(\omega_{s,i}t)$, but a more accurate statistical representation of the turbulence is preferred. These can be obtained from analysis of the unsteady forces on the body or the near wake using techniques such as fast Fourier transforms. Within the model, fluctuation magnitudes $C'_{\zeta,i}(\alpha,\beta)$ are obtained from look-up tables or equations similar to process applied in the determination of the quasi-steady mean flow aerodynamic coefficients. The primary shedding frequency, ω_s, (or the higher frequencies) can also be evaluated from quasi-steady or dynamic simulations or tests. Different forms of the fluctuation function, ϕ, are assessed later in the paper.

MODEL VERIFICATION AND VALIDATION

Comparison with URANS CFD Computations

Table 2: Operating conditions for validation case for the CONEX rectangular box

Mass (kg)	1.49	**Initial roll** (deg.)	0.0
$\boldsymbol{I_{xx}}$ (10^{-3} kgm^2)	7.77	**Initial pitch** (deg.)	-8.8
$\boldsymbol{I_{yy}}$ (10^{-3} kgm^2)	11.04	**Initial yaw** (deg.)	0.0
$\boldsymbol{I_{xx}}$ (10^{-3} kgm^2)	10.49	$\boldsymbol{U_\infty}$ (mph)	25

The reduced-order aerodynamic model has been validated by comparison with URANS computations with a 1/11th-scale CONEX container suspended by a tether in a wind tunnel. These results are also compared with URANS computations and wind tunnel data first published by Rosen et al. (Ref. 37). The operation or "flight" conditions for this case are listed in Table 2.

To validate the reduced-order model, the aerodynamic results from URANS computations are applied as the input to the dynamic equations of motion, which permits a direct comparison between the reduced-order and URANS aerodynamics. Figure 5(a) compares the URANS and reduced-order yaw moment predictions for this case, without including the vortex shedding terms of Eq. 7 in the reduced-order model. Both the quasi-steady and unsteady aerodynamic predictions, the latter including the effects of the dynamic filter, are presented. The reduced-order model accurately reproduces the time-averaged URANS yaw moment, and the difference between the quasi-steady and unsteady yaw moment is small in this case. This proximity is not unexpected, as the reduced frequency of the yaw oscillation is only 0.053, and only very small changes from quasi-steady aerodynamics are expected in this range (refer to Fig. 4). However, even these small unsteady effects can have a significant impact on dynamic stability. The frequency content from URANS and the reduced-order model was extracted using a Fast Fourier Transform (FFT) and is examined in Fig. 6(a). The reduced-order model lacks much of the higher frequency content in the URANS simulation when no shedding terms are included.

Figure 5(c) presents the reduced-order yaw moment prediction including the first vortex shedding harmonic $\phi(\omega_{s,1},t)$ modeled as $\sin(\omega_{s,1}t)$ where $N = 1$ in Eq. 7. $C'_{\zeta,1}(\alpha,\beta)$ is constructed in quasi-linear form from static simulations, in the same manner that the quasi-steady aerodynamics are determined. This simple harmonic approximation of the shedding terms reproduces some of the higher harmonic content from URANS computations, but it is comparatively more periodic.

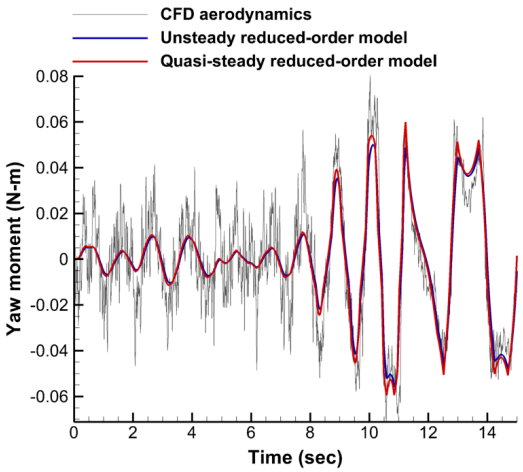

(a) Without vortex shedding terms

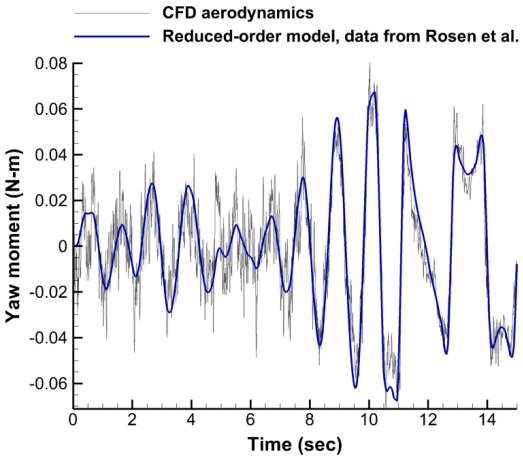

(b) Using quasi-steady data from (Ref. 37)

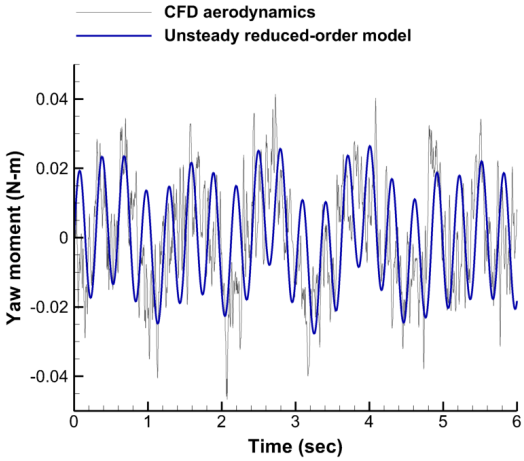

(c) With simple harmonic shedding terms

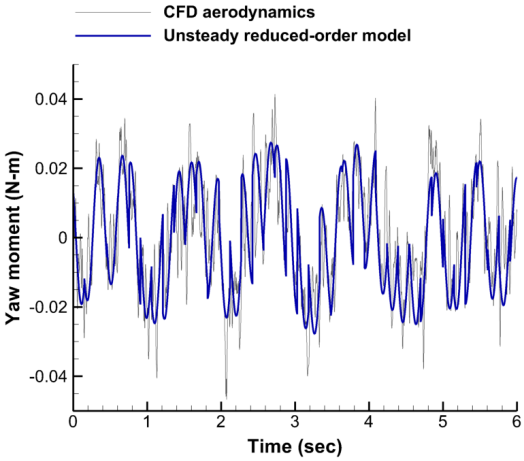

(d) Shedding terms with phases matched to CFD

Fig. 5: Comparison of reduced-order yaw moment with full CFD yaw moment

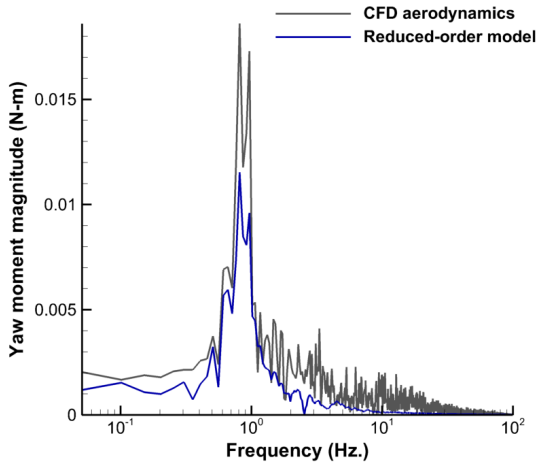

(a) Without vortex shedding terms

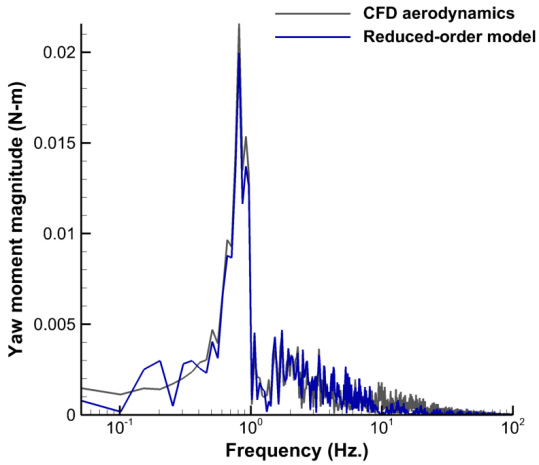

(b) Shedding terms with phases matched to CFD

Fig. 6: Frequency content of yaw moment for CFD and reduced-order model

The higher harmonic content in the URANS originates from the large eddies captured by the hybrid RANS-LES turbulence approach, which are chaotic by comparison.

As the frequency and magnitude of the fluctuations accurately represent the URANS result, it is possible to reproduce the chaotic nature of the turbulent vortex shedding process by varying the phase of each fluctuation. The purpose of this process is to deduce an appropriate form of the function $\phi(\omega_{s,i},t)$ that accurately represents the vortex shedding fluctuations observed in simulations and experiments. In practice, this process is performed by overlaying the URANS C'_ζ fluctations on the reduced-order prediction of $\overline{C_\zeta}$ and evaluating the phase of each fluctuation relative to the simple harmonic representation $\sin(\omega_{s,1}t)$. This phase information is then employed to determine a representative probability distribution function. The result of the phase-determination procedure, applied to the validation case, is presented in Fig. 5(d), which is a much more accurate representation of the vortex shedding behavior than a simple harmonic model. Figure 6(b) presents the frequency-domain representation of this data compared with the frequency content of the URANS yaw moment CFD data. Despite the fact that only a single shedding term is included, the phase-determination process results in nearly identical frequency content between URANS CFD and the reduced-order model over a broad range of frequencies from 0.5 to 10 Hz.

In addition to evaluating the reduced-order yaw moment with quasi-steady data drawn from URANS CFD simulations, the performance of the model was also examined with data from an external source. Figure 5(b) compares the unsteady reduced-order yaw moment, without vortex shedding terms, with quasi-steady data taken from wind tunnel experiments (Ref. 37). These tunnel experiments were performed at a somewhat lower Reynolds number, but the time-averaged trace closely matches the unsteady URANS computations, albeit with some overshoots. In the wind tunnel experiments, reattachment behavior was observed at a similar yaw angle as in the static URANS computations but with a larger yaw moment coefficient, which accounts for the differences in magnitude between the blue curves in Figs. 5(a) and (b). Some differences are to be expected from two different data sets, but the result presented here demonstrates that the model is robust with respect to the source of quasi-steady data. Data from computations, wind tunnel experiments, or flight tests can all be used for the reduced-order model, and variations in test conditions are not a significant concern for a sharp-edged configuration as long as the flow regimes are similar.

Vortex Shedding Model

Of course, it is not practical to match the shedding phases in the reduced-order model with high-fidelity computations for every case, nor is that the intention of the model. Instead, a limited number of samples may be used to establish an expected vortex shedding distribution that may be randomized in the reduced-order model to mimic the chaotic nature of turbulence. To this end, two additional URANS simulations were performed with the same freestream speed of 25 mph but with different initial conditions. The phases of the yaw moment fluctuations from the three simulations were then fit with a normal distribution, illustrated in Fig. 7. The best-fit distribution has a mean $\mu = 3.14$ and a standard deviation $\sigma = 1.62$, and was incorporated in the shedding model as

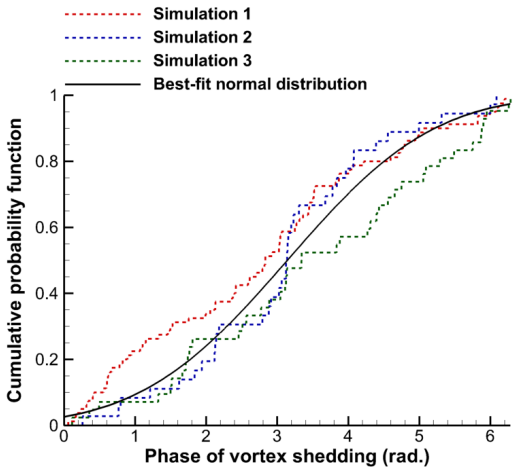

Fig. 7: Shedding phases from three separate simulations fit a normal distribution

$$\phi(\omega_s,t) = \sin[\omega_s t + \mathrm{rand_n}(\mu,\sigma)], \tag{8}$$

where $\mathrm{rand_n}(\mu,\sigma)$ is a random number drawn π/ω_s seconds from a normal distribution whose probability density function is given by

$$f(x,\mu,\sigma) = \frac{1}{\sigma\sqrt{2\pi}} e^{-\frac{(x-\mu)^2}{2\sigma^2}}. \tag{9}$$

This algorithm derived from the best-fit distribution was then applied for the remainder of the simulations as representative of the average shedding characteristics.

RESULTS

Dynamic simulations with the reduced-order model have been performed for several different applications and compared with equivalent URANS simulations or test data, as warranted.

1/11th-Scale CONEX Rectangular Container

Several simulations were performed for the CONEX rectangular container geometry to compare the dynamics of the reduced-order model with URANS. The first case applied the same operating conditions as were presented in the validation case (Table 2), but now the reduced-order model provided the aerodynamic forcing function to the 6-DoF system. Two variations of this case have been considered: first, the quasi-steady data were taken directly as the time-averaged coefficients $\overline{C}_\zeta$; second, the quasi-steady coefficients were passed

through the dynamic filter of Eq. 3 to produce the time-averaged coefficients. In both variations, shedding terms were added using the form given in Eq. 8. The only difference between the two is the manner in which the time-averaged coefficients have been computed.

Figure 8 compares the yaw dynamics for the two variations of this case. In the URANS simulation, yaw oscillations increased over time until the box eventually rotated more than 90 degrees in yaw. When applying quasi-steady aerodynamics (Fig. 8(a)), the yaw oscillations grew but reached a limit cycle and the rotation never occurred. With unsteady aerodynamics, the yaw oscillations continued to increase in magnitude and rotation occurred at a time of 14 seconds. Notably, the rotation occurred in the same direction and within two seconds of the URANS prediction. The particular set of randomly sampled shedding phases had an influence on the amount of time for and direction of rotation. With the reduced-order model, this rotation consistently occurred when using unsteady aerodynamics, but it was never observed with only quasi-steady aerodynamics, no matter what shedding phases were applied. This comparison highlights the importance of the inclusion of the unsteady aerodynamic terms in the reduced-order model. Though Fig. 5 indicated that the phase lag of the unsteady model is small in this case, even this small phase lag reduces the effective damping of the system and produces yaw divergence.

A second test case was evaluated with the rectangular box geometry to assess the performance of the reduced-order model at a different flight speed. The same geometry and mass parameters were applied as inputs (Table 2), but $\boldsymbol{U}_\infty$ was increased to 40 mph with an initial pitch angle of 0 degrees. The higher flight speed and new initial condition resulted in larger aerodynamic forces and moments on the tethered container. As a result, the URANS simulation predicted rapid yaw divergence, compared to the 25 mph case where a number of oscillations were required before the yaw angle built up sufficiently. The URANS yaw angle time history is presented in Fig. 9. After yaw divergence occurred, the load continued to spin counterclockwise for several rotations, briefly stopped spinning, and then began spinning again. The spinning behavior in Fig. 9 is identified by a continuously increasing or decreasing yaw angle, eventually jumping from 180° to -180°, or vice versa, as the yaw angle is defined in the range $\beta \in (-\pi, \pi]$.

When evaluating this case with quasi-steady aerodynamics only, yaw divergence never occurred. Instead, yaw oscillations initially grew in size but quickly reached a limit cycle, as demonstrated in Fig. 9(a), the same behavior observed for the 25 mph case. In contrast, when the full unsteady aerodynamic reduced-order model was applied, yaw divergence and spinning behaviors occurred more quickly than in the 25 mph simulation (Fig. 9(b)). The direction of spinning motion in the reduced-order simulation was opposite that of the CFD simulation, but the direction was highly dependent on the chaotic turbulent vortex shedding and may switch from one trial to the next, as noted in prior tests (Ref. 38); the important result is the behavior rather than the direction. This result confirms the major finding of the 25 mph case; namely, that the phase lag and magnitude attenuation induced by unsteady aerodynamics and modeled by Eq. 3 are important to correctly predict the stability characteristics of tethered loads.

The reduced-order model is capable of capturing the yaw dynamics of fully-coupled URANS and 6-DoF computations. At the 40 mph flight speed, both URANS and the reduced-order model predicted large yaw oscillations and eventual spinning motion of the tethered load. The spin rate is not constant but varies with yaw angle. Spin rates were averaged over three cycles for both simulations (Fig. 10). A 31% higher average yaw rate was realized in the reduced-order model, but the variations of yaw rate with yaw angle were similar, both in terms of phase and magnitude. The average phase difference between the URANS and reduced-order yaw rate, measured at the eight local minima and maxima in Fig. 10, was 8.1 degrees with a standard deviation of 4.0 degrees. The difference between the maximum and minimum yaw rate was 15% smaller in the reduced-order simulation than in URANS.

The differences in mean yaw rate and the amount of time required for spinning to occur merit further discussion. Figure 11 compares the yaw moment from the reduced-order model and URANS when URANS dynamics are imposed, without the shedding terms in the reduced-order model. The comparison procedure is the same as was used for the validation case in Fig. 5(a). Here both the quasi-steady and unsteady reduced-order predictions overestimate the maximum yaw moment during some portions of the time history. This deficiency points to the fact that the quasi-steady data are not complete; recall that the quasi-steady model is in quasi-linear form. In the linearization, the angle of attack was held constant at $\alpha = 0$ while the yaw angle was varied, but in the 40 mph simulation the angle of attack became large while yaw rotation also occurred. The reduced maximum yaw moment at higher angle of attack reduces the yaw stiffness. As a result, yaw rotation occurred more quickly in URANS than in the reduced-order simulation, and the spin rate was also affected. These discrepancies can be avoided with more comprehensive quasi-steady data.

In the case of rectangular prisms such as the CONEX container, there exist empirical relations in the literature to predict the quasi-steady forces and moments, both in pure yaw or angle of attack and in coupled orientation (Refs. 6, 12). In future work, these approaches will be used to augment the quasi-steady data for this geometry and the performance of the model will be re-evaluated at the higher angles of attack where the current data set is lacking.

Figure 12 depicts the trailing angle (the angle that the cable makes with the vertical in the $x-z$ plane) during the 25 mph and 40 mph simulations. Results from the reduced-order model are shown here using both quasi-steady and unsteady aerodynamics (both included vortex shedding fluctuations). In the 25 mph simulation, there were initially small oscillations in the trailing angle, as the initial condition was set so that the aerodynamic and gravitational forces would be nearly balanced. When the box rotated in yaw, the trailing angle in-

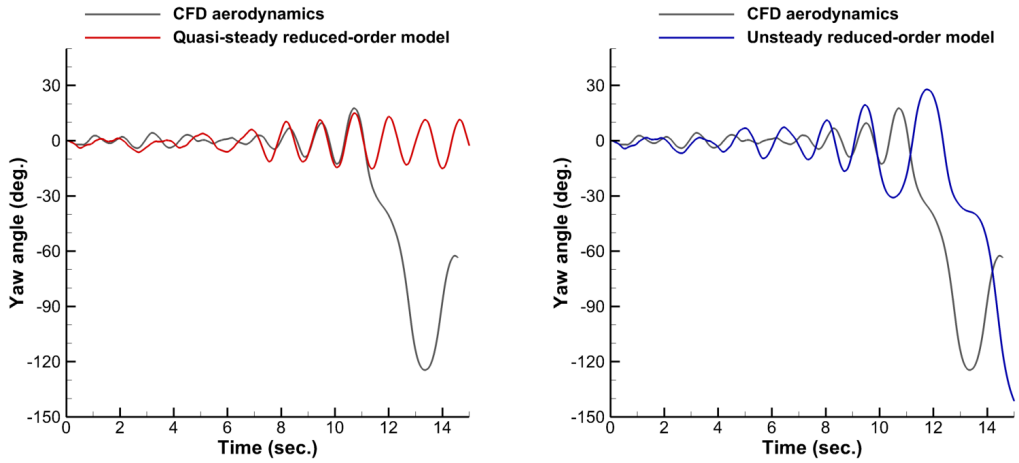

(a) Quasi-steady aerodynamics (b) Unsteady aerodynamics

Fig. 8: Comparison of yaw dynamics for URANS and reduced-order simulations for the rectangular box at 25 mph

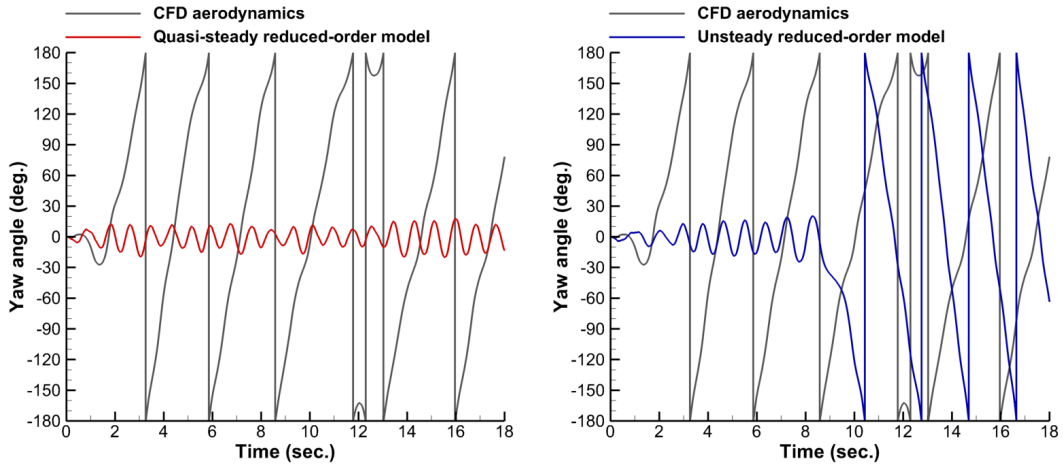

(a) Quasi-steady aerodynamics (b) Unsteady aerodynamics

Fig. 9: Comparison of yaw dynamics for URANS and reduced-order simulations for the rectangular box at 40 mph

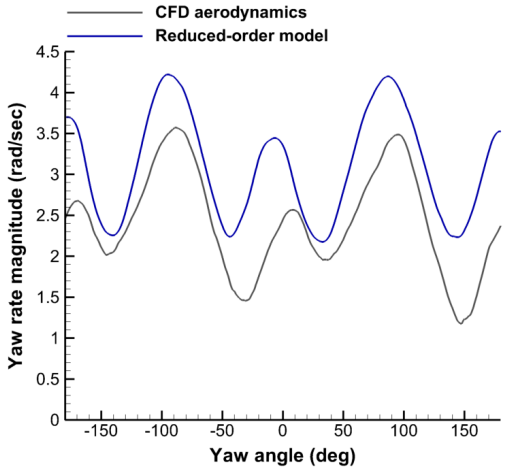

Fig. 10: Yaw rate comparison for 40 mph case

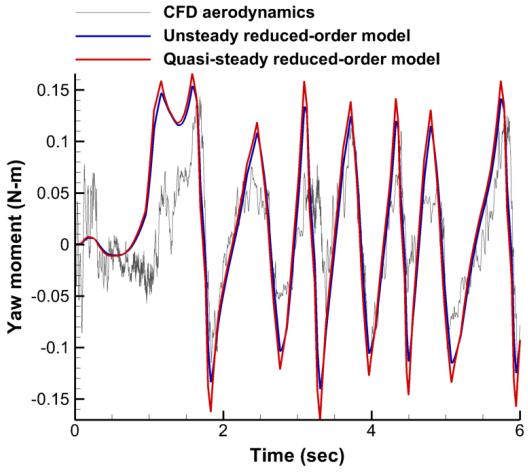

Fig. 11: Yaw moment comparison for 40 mph case

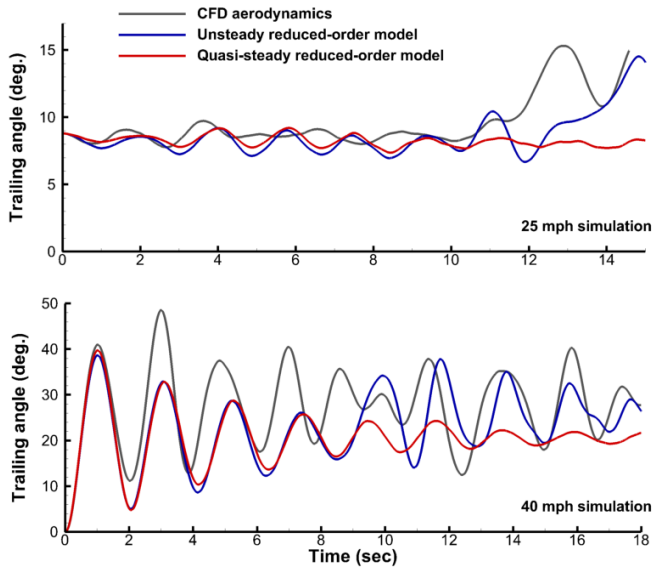

Fig. 12: Trailing angle comparisons between URANS and the reduced-order model for the rectangular box at 25 mph and 40 mph

creased significantly because the broad side had turned into the flow. The quasi-steady model did not predict this yaw rotation, so the trailing angle remained small. Before yaw rotation occurred, the mean trailing angle from URANS was 8.6°, whereas it was 8.2° for both forms of the reduced-order model, representing a 4.6% error. In wind tunnel experiments performed by the Experimental Aerodynamics and Concepts Group at Georgia Tech, the trailing angle for this 25 mph case was observed as 9° (Ref. 17), which agrees closely with the simulations presented here.

In the 40 mph URANS simulation, yaw rotation occurred almost immediately and then spinning commenced. With the unsteady reduced-order model, yaw rotation occurred later; with quasi-steady aerodynamics it never occurred. The unsteady reduced-order model accurately predicted the trailing angle in the 40 mph case; the mean trailing angle was 25.9° in the unsteady reduced-order model following yaw rotation, compared to 28.1° in URANS, resulting in an error of 7.8%. In contrast, the mean trailing angle for the quasi-steady case (in which yaw rotation never occurred) was only 20.6°, resulting in an error of 26.7%. The trailing angle comparison reinforces the conclusion that unsteady aerodynamic phenomena may be very important in tethered load dynamics, even when the reduced frequency is small.

Cylindrical Load in Accelerating Flight

The reduced-order aerodynamic model has been incorporated into the Georgia Tech UAV Simulation Tool (GUST) (Ref. 39) by the UAV Research Facility at Georgia Tech for tethered-load simulations. The GUST framework is employed in simulation to develop and test control algorithms for guidance of the helicopter and tethered load before implementing them in UAVs. The realism of the reduced-order aerodynamic model for the tethered load is important in minimizing the amount of time iterating on the control law parameters between simulation and flight tests. The reduced-order aerodynamic model for tethered loads presented in this effort and now implemented in GUST represents a significant increase in fidelity over the previous model, which considered only quasi-steady drag (Ref. 40).

Preliminary flight tests were performed by the UAV Research Facility using a cylindrical tethered load with a diameter of 0.28 meters, a length of 0.26 meters, and mass of 5.2 kg. It was attached by a single tether to one of the flat ends of the cylinder and on the other end to the GTMAX unmanned helicopter; the tether had a length of 14.0 meters. The GTMAX helicopter flew a manuever in which it was commanded to accelerate at a rate of 2.0 ft/s^2 (0.61 m/s^2) from a low speed up to a maximum speed of 20 ft/s (6.1 m/s), hold that speed for five seconds, and then decelerate at 2.0 ft/s^2 until stationary. The actual flight speed profile recorded by the onboard sensors during this maneuver is provided in Fig. 13(a).

Quasi-steady aerodynamic data has been compiled from numerical simulations to permit dynamic simulation of cylindrical tethered loads using the reduced-order aerodynamic model presented in this work. The flight speed profile depicted in Fig. 13(a) was taken as a prescribed input to the simulation by applying this velocity profile to the fixed attachment point of the tether opposite the cylinder. The wind speed was zero in the simulation. An alternative approach of applying the flight speed profile as a variable wind velocity in the simulation while holding the tether attachment point fixed was considered, but that approach was rejected because it omits inertial forces arising from helicopter acceleration.

The GTMAX helicopter has an onboard visual state estimation system for the load via a downward-facing camera. The images from the camera are processed by an onboard computer and used for control purposes. Figure 13(b) presents the measured and simulated load positions in the image plane during this maneuver. The sign convention is such that a positive x-position in the image plane indicates that the load is behind the helicopter in the longitudinal plane, while a positive y-position means that the load is to the right of the helicopter in the lateral plane. The load lags behind the helicopter during the first part of the manuever while the helicopter is accelerating, and during the second half of the maneuver it moves out in front. The load also undergoes pendulum-like oscillations in the lateral plane throughout the maneuver.

The overall magnitudes of motion in x and y for the load on the image plane are similar between flight test and simulation, though the positions are not always the same at the same time. Note, however, that the instantaneous position of the load is sensitive to the initial conditions, turbulent shedding effects, and wind gusts. The flight test data presented here contains some uncertainty due to signal dropouts and unmeasured wind turbulence, which could not be properly accounted for given the time and weather constraints on the flight tests. As a result, the initial conditions could not be ascertained to a high degree of confidence. Nonetheless, the simulation produces

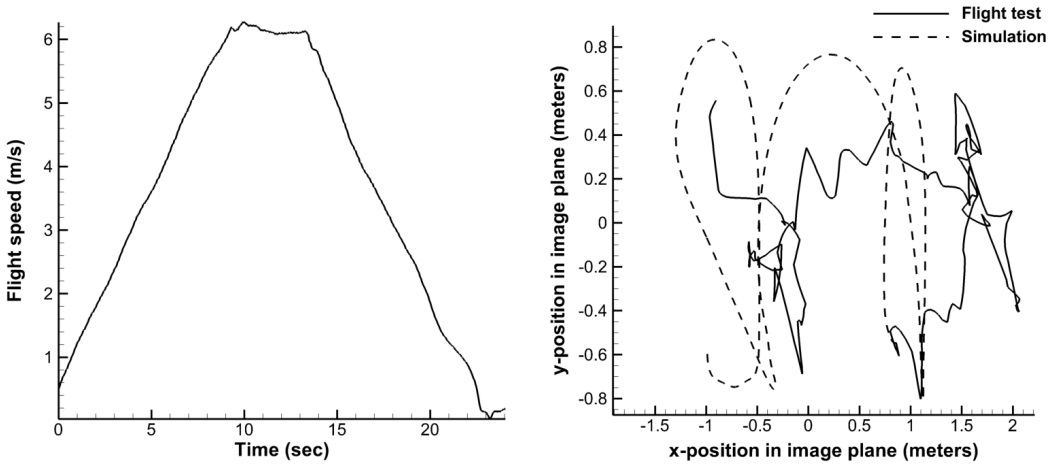

(a) Measured flight speed profile

(b) Tethered load position on image plane

Fig. 13: Flight test data and comparison with simulation for a cylindrical tethered load

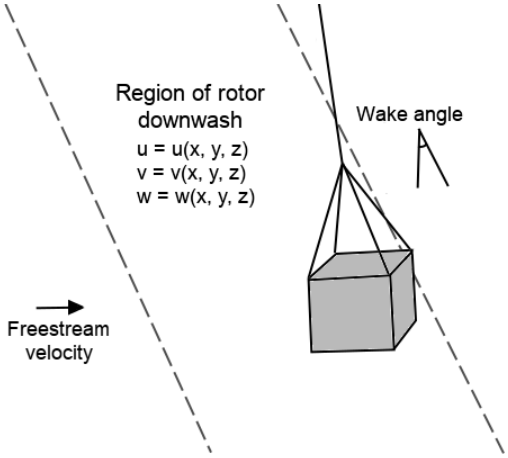

Fig. 14: Illustration of a rotor downwash model

the correct behavior if wind gusts are neglected, as noted by the general trends in Fig. 13(b). Wind gusts introduce perturbations to the state of the load and uncertainty in reproducing the exact position with time during simulation. Additional flight tests are planned in the near future for further validation of the aerodynamic model. These tests will incorporate permutations of the flight speed profile, and the weight of the cylinder will be reduced to decrease the magnitude of gravitational and inertial forces relative to the aerodynamic forces.

EXTENDING THE MODEL

A significant benefit of this reduced-order model is that it can be readily extended to incorporate external effects such as rotor downwash, atmospheric boundary layers, and wind tunnel walls. Each of these effects may be modeled as a modification of the background velocity field $\boldsymbol{U}_\infty$, and their influences on tethered load dynamics can be quickly assessed. In contrast, with the URANS approach such studies would be very costly and require modifications to the boundary conditions or the inclusion of additional viscous surfaces (i.e. rotor blades).

Rotor Downwash and Atmospheric Boundary Layers

The impacts of rotor downwash and atmospheric boundary layers are straightforward to incorporate because the velocity field is independent of the tethered load. An illustration of a model for incorporating rotor downwash is presented in Fig. 14. The downwash field itself must be drawn from external data from testing or computations. For example, Talbot et al. (Ref. 41) model the rotor downwash as the following empirical function of wake angle:

$$\frac{w}{v_i} = \sum_{n=0}^{4} k_n \chi^n, \tag{10}$$

where v_i is the rotor-induced velocity predicted by momentum theory. The wake angle, χ, is a function of advance ratio and inflow ratio, $\chi = \tan^{-1}\left(\frac{\mu}{\lambda}\right)$, and the coefficients k_n vary with position in the rotor wake. The wake angle and values of the coefficients are referenced to the plane in which the wake's axis lies, which is determined by the direction of motion of the helicopter. In this model, the tethered load may be considered to be within the influence of the wake if its center of gravity is within the region shown in Fig. 14, or partial contributions of the downwash may be assumed when only parts of the load are within this region. Empirical approximations of swirl within the wake region may also be modeled.

The effects of atmospheric turbulence may also be simulated via modification of the background velocity field. One possible choice is the seminal Dryden wind turbulence model (Ref. 42). In this model, atmospheric turbulence is assumed to be variable in space, following a stochastic distribution, but constant in time. Gusts are encountered when a vehicle flies through this spatially-varying field at a given speed. The assumption employed in this representation is that the temporal scales of these features are much larger than the

time it takes to fly through them. The spatial variations are characterized by turbulence spectra in three directions:

$$\Phi_u(\Omega) = \sigma_u^2 \frac{2L_u}{\pi} \frac{1}{1+(L_u\Omega)^2} \tag{11}$$

$$\Phi_v(\Omega) = \sigma_v^2 \frac{2L_v}{\pi} \frac{1+12(L_v\Omega)^2}{\left[1+4(L_v\Omega)^2\right]^2}$$

$$\Phi_w(\Omega) = \sigma_w^2 \frac{2L_w}{\pi} \frac{1+12(L_v\Omega)^2}{\left[1+4(L_w\Omega)^2\right]^2},$$

where L_i is a length scale related to velocity fluctuation i, σ_i is the turbulence intensity, and Ω is the spatial frequency of the gust. The Dryden model is an example of a continuous gust model, which assumes gusts are random and can be represented by a normal distribution, among other assumptions (Ref. 43). Alternatively to the Dryden model or other continuous gust models, discrete gust models are sometimes used to determine the response to a single atmospheric disturbance. Discrete gusts are usually represented by a sinusoidal curve which varies spatially with maximum amplitude dictated by FAA regulations.

Wind Tunnel Walls

The effects of wind tunnel walls can also be modeled as a variation of the velocity field $\boldsymbol{U}_\infty$. Wind tunnel walls have been implied by Sharma et al. (Ref. 16) to have an impact on tethered load dynamics. Their wall-effect model was formulated in two dimensions with a single doublet representing the tethered load, and walls were modeled using the method of images. The underlying assumption in this approach is that wall effects may be incorporated via potential flow theory. A 6-DoF simulation including wall effects can be accomplished using a similar approach, but three-dimensional elements (surfaces instead of points or panels) are needed to discretize the walls and tethered load. The method of images may still be used; however, this method can become complicated when multiple walls are involved or when the walls are curved. A preferred approach to the method of images is to direcretize the wind tunnel walls themselves by a number of source surfaces. In either case, the strengths of the potential-flow surface elements are determined by applying the inviscid slip boundary condition and solving a system of equations. The induced velocity from wall effects acting on the tethered load may then be determined by superposition of the influences of all surface elements. The resolution of the geometry discretization by these elements determines the fidelity of the wall effect calculation.

COMPUTATIONAL COST

The computational cost of the reduced-order model is significantly less than that of coupled URANS and 6-DoF simulation. For the 25 mph rectangular box case detailed previously, the URANS simulation required 50,000 steps for 15 seconds of dimensional time. The 50,000 steps needed approximately 625 hours on 128 cores of a Cray XE6 cluster, each core rated at 2.5 GHz, for a total cost of 80,000 CPU-hours. In contrast, the same 50,000 steps for the reduced-order simulation required 14.1 minutes on a single processor rated at 2.33 GHz, for a total cost of 0.24 CPU-hours. The cost ratio between the two approaches is over five orders of magnitude in CPU-hours and over three orders of magnitude in actual time. The large discrepancy highlights why the URANS approach may be too expensive for stability and sensitivity analysis needed for tethered loads.

Additional cost savings can be realized with the reduced-order model. To date, the reduced-order model has been implemented in MATLAB, and it has not been optimized for speed. Recoding with a compiled computer language should decrease the cost significantly. Additionally, since the reduced-order model does not need to resolve turbulent flow features (it only models their effects), the time step can be increased significantly compared to an equivalent URANS simulation. However, some stability restrictions do apply to the numerical integration of the 6-DoF equations of motion, and preliminary tests have indicated that the dynamic filter for unsteady aerodynamics further restricts the time step size.

CONCLUSIONS

This paper presents a novel, physics-based reduced-order model for simulation of tethered-load dynamics. The model is a combination of quasi-steady aerodynamics, unsteady effects of body motion, and fluctuations from turbulent vortex shedding. One of the main priorities in creating the model has been to maintain a firm physical basis. For example, the unsteady aerodynamic model draws on classical unsteady aerodynamics theory and is formulated in a manner that is similar to successful dynamic stall models. The vortex shedding effects implemented in the model are based on observed characteristics from high-fidelity numerical simulations; these vary with angle of attack and yaw, and their behavior in time is chaotic in nature. Global nonlinearities are captured via lookup tables for quasi-steady aerodynamics.

The reduced-order model is evaluated by comparisons with URANS simulations of tethered-load dynamics for two common geometry types. The important findings are listed below:

- Quasi-steady aerodynamics alone is shown to be insufficient for accurate prediction of tethered-load stability characteristics, even when the reduced frequency of body motion is small.
- The reduced-order model accurately predicts the time-averaged and fluctuating components of the aerodynamic loading for given kinematics.
- In dynamic simulation of a CONEX tethered load, the reduced-order model predicts correct stability characteristics.
- Computational cost is reduced by several orders of magnitude compared to the URANS simulation approach.

- The model is robust in that quasi-steady data can be drawn from a number of sources including flight testing, wind tunnel experiments, and computations.
- The modeling approach is scalable and applicable to bluff body dynamics in general. It is only necessary to change the quasi-steady aerodynamic data for new geometries.
- Extending the model to include effects of rotor downwash, atmospheric turbulence, or wind tunnel walls is straightforward and does not significantly increase cost.

Improvements and further development to the reduced-order model are possible in future work. These improvements are as follows:

- The quasi-steady data for the rectangular container can be augmented using empirical relations available in the literature to remove the need for the quasi-linear assumption in the model.
- The unsteady aerodynamics in the model is based on classical potential flow unsteady theory. This model has been demonstrated to correctly predict the behavior of the tethered load in the cases considered here, but it will be important to assess it in more extreme cases near the limit of stability and possibly to develop modifications appropriate for separated viscous flow.
- The vortex shedding model assumes a constant Strouhal number, eliminating the possibility of vortex shedding lock-in with body dynamics frequencies. Future work may extend the model to incorporate this phenomenon.

ACKNOWLEDGEMENTS

This research is funded through the U.S. Army/Navy/NASA Vertical Lift Rotorcraft Center of Excellence at Georgia Tech under Task 10 "Dynamic-Aerodynamic Interactions of Bluff Bodies: Computational Investigations" under the direction of Mahendra Bhagwat of AFDD, Agreement No. W911W6-11-2-0010. The authors would like to thank the technical points of contact of this project, Marty Moulton and Tom Thompson of AMRDEC for their insights, as well as noted researchers in the area of sling loads: Luigi Cicolani, Doug Greenwell, and Aviv Rosen.

The authors would also like to thank the UAV Research Group at Georgia Tech for their collaboration in implementing the reduced-order aerodynamic model in their simulator and for the use of their flight test data.

The U.S. Government is authorized to reproduce and distribute reprints notwithstanding any copyright notation thereon. The views and conclusions contained in this document are those of the authors and should not be interpreted as representing the official policies, either expressed or implied, of the U.S. Government.

REFERENCES

[1]Modi, V. and Slater, J., "Unsteady Aerodynamics and Vortex Induced Aeroelastic Instability of a Structural Angle Section," *Journal of Wind Engineering and Industrial Aerodynamics*, Vol. 11, (1–3), May 1983, pp. 321–334.

[2]Matsumoto, M., Shiraishi, N., and Shirato, H., "Rain-Wind Induced Vibration of Cables and Cable-Stayed Bridges," *Journal of Wind Engineering and Industrial Aerodynamics*, Vol. 41–44, 1992, pp. 2011–2022.

[3]Zaki, T., Sen, M., and Gad-el Hak, M., "Numerical and Experimental Investigation of Flow Past a Freely Rotatable Square Cylinder," *Journal of Fluids and Structures*, Vol. 8, (7), 1994, pp. 555–582.

[4]Matsumoto, M., "Vortex Shedding of Bluff Bodies: A Review," *Journal of Fluids and Structures*, Vol. 13, (7–8), October 1999, pp. 791–811.

[5]Cheng, M. and Liu, G., "Effects of Afterbody Shape on Flow around Prismatic Cylinders," *Journal of Wind Engineering and Industrial Aerodynamics*, Vol. 84, (2), January 2000, pp. 181 – 196.

[6]Greenwell, D., "Modelling of Static Aerodynamics of Helicopter Underslung Loads," *The Aeronautical Journal*, Vol. 115, (1166), April 2011, pp. 201–219.

[7]Raz, R., Rosen, A., Carmeli, A., Lusardi, J., Cicolani, L. S., and Robinson, L. D., "Wind Tunnel and Flight Evaluation of Stability and Passive Stabilization of Cargo Container Slung Load," Proceedings of the 64th American Helicopter Society Annual Forum, April 29 – May 1, 2008.

[8]Matheson, N., "The Stability of Portable Bridges Carried on Slings Beneath Helicopters," Technical Report 154, Defence Science and Technology Organisation, 1980.

[9]Raz, R., Rosen, A., Carmeli, A., Lusardi, J., Cicolani, L. S., and Robinson, L. D., "Wind Tunnel and Flight Evaluation of Passive Stabilization of a Cargo Container Slung Load," *Journal of the American Helicopter Society*, Vol. 55, (3), July 2010.

[10]Cicolani, L. S., Raz, R., Rosen, A., Gordon, R., Cone, A., Theron, J. N., Lusardi, J., Tischler, M., and Robinson, M. D., "Flight Test, Simulation and Passive Stabilization of a Cargo Container Slung Load in Forward Flight," Proceedings of the 63rd American Helicopter Society Annual Forum, May 1–3, 2007.

[11]Raz, R., Rosen, A., Cicolani, L. S., Lusardi, J., Gassaway, B., and Thompson, T., "Using Wind Tunnel Tests for Slung Loads Clearance," Proceedings of the 67th American Helicopter Society Annual Forum, May 3–5, 2011.

[12]Prosser, D. T. and Smith, M. J., "Characterization of Flow Around Rectangular Bluff Bodies at Angle of Attack," *Physics Letters A*, Vol. 376, (45), 2012, pp. 3204 – 3207.

[13]Cicolani, L. S. and Kanning, G., "Equations of Motion of Slung Load Systems with Results for Dual Lift," Technical Report NASA TM-102246, 1990.

[14]Cicolani, L. and da Silva, G., J, "Unsteady Aerodynamic Model of a Cargo Container for Slung-Load," *The Aeronautical Journal*, Vol. 108, (1085), July 2004, pp. 357–368.

[15]Cone, A. C., *Simulation of a Cargo Container Slung Load at Speeds with Signficiant Aerodynamic Effects*, Master's thesis, California Polytechnic State University, 2007.

[16]Sharma, S., Raghav, V., Komerath, N., and Smith, M., "Efficient Modeling of Dynamic Blockage Effects for Unsteady Wind Tunnel Testing," Proceedings of the 69th American Helicopter Society Annual Forum, May 20–24 2013.

[17]Prosser, D. T. and Smith, M. J., "Navier-Stokes-Based Dynamic Simulations of Sling Loads," Paper AIAA-2013-1922, Proceedings of the 54th AIAA/ASCE/AHS/ASC Structures, Structural Dynamics, and Materials Conference, April 8 – April 11 2013.

[18]Peters, D. and Johnson, M., "Finite-State Airloads for Deformable Airfoils on Fixed and Rotating Wings," Proceedings of the Symposium n Aeroelasticity and Fluid/Structure Interaction, Americal Society of Mechanical Engineers Winter Annual Meeting, November 1994.

[19]Ahaus, L. A. and Peters, D. A., "Unified Airloads Model for Morphing Airfoils in Dynamic Stall," Proceedings of the American Helicopter Society Specialist's Conference on Aeromechanics, January 20–22 2010.

[20]Ahaus, L., Liggett, N., Peters, D. A., and Smith, M. J., "Unsteady Aerodynamics of Single and Multi-Element Airfoils," Proceedings of the 36th European Rotorcraft Forum, September 7–9 2010.

[21]Forbes, A., Pirau, S., Liberi, B., Raghav, V., and Komerath, N., "Testing-Based Approach to Determining the Divergence Speed of Slung Loads," Proceedings of the 70th American Helicopter Society Annual Forum, May 20–22, 2014.

[22]Martin, J. D. and Simpson, T. W., "Use of Kriging Models to Approximate Deterministic Computer Models," *AIAA Journal*, Vol. 43, (4), September 2005, pp. 853–863.

[23]Glaz, B., Friedmann, P., Liu, L., Cajigas, J. G., and Sankar, L. N., "Reduced-Order Dynamic Stall Modeling with Swept Flow Effects Using a Surrogate-Based Recurrence Framework," *AIAA Journal*, Vol. 51, (4), April 2013.

[24]Hoerner, S., *Fluid-Dynamic Drag*, Hoerner Fluid Dynamics, Midland Park, NJ, 1958.

[25]Sakamoto, H. and Haniu, H., "A Study on Vortex Shedding from Spheres in a Uniform Flow," *Journal of Fluids Engineering*, Vol. 112, (4), category:bluff bodies, December 1990, pp. 386–392.

[26]Theodorsen, T., "General Theory of Aerodynamic Instability and the Mechanism of Flutter," Technical Report NACA 496, 1935.

[27]Harris, F. D., *Introduction to Autogyros, Helicopters, and Other V/STOL Aircraft, Vol. I: Overview and Autogyros*, NASA Technical Information Service, Springfield, VA, 2012.

[28]Smith, M. J., Liggett, N. D., and Koukol, B. C., "Aerodynamics of Airfoils at High and Reverse Angles of Attack," *AIAA Journal of Aircraft*, Vol. 48, (6), November–December 2011, pp. 2012–2023.

[29]Lynch, C. E. and Smith, M. J., "Extension and Exploration of a Hybrid Turbulence Model on Unstructured Grids," *AIAA Journal*, Vol. 49, (11), November 2011, pp. 2585–2590.

[30]Shenoy, R., Smith, M., and Park, M., "Unstructured Overset Mesh Adaptation with Turbulence Modeling for Unsteady Aerodynamic Interactions," *Journal of Aircraft*, Vol. 51, (1), January 2014.

[31]Zdravkovich, M., Brand, V., Mathew, G., and Weston, A., "Flow Past Short Cylinders with Two Free Ends," *Journal of Fluid Mechanics*, Vol. 203, June 1989, pp. 557–575.

[32]Bisplinghoff, R., Ashley, H., and Halfman, R., *Aeroelasticity*, Addison-Wesley Publishing Company, Inc, 1955.

[33]Leishman, J. G., *Principles of Helicopter Aerodynamics*, Cambridge University Press, Cambridge, second edition, 2006.

[34]Johnson, W., *Rotorcraft Aeromechanics*, Cambridge University Press, Cambridge, 2013.

[35]McAlister, K., Lambert, O., and Petot, D., "Application of the ONERA Model of Dynamic Stall," Technical Report NASA TP 2399, 1984.

[36]Cicolani, L. S., Cone, A., Theron, J., Robinson, L. D., Lusardi, J., Tischler, M. B., Rosen, A., and Raz, R., "Flight Test and Simulation of a Cargo Container Slung Load in Forward Flight," *Journal of the American Helicopter Society*, Vol. 54, (3), July 2009, pp. 1–18.

[37]Rosen, A., Cecutta, S., and Yaffe, R., "Wind Tunnel Tests of Cube and CONEX Models," Technical Report TAE 844, Technion – Institute of Technology, Faculty of Aerospace Engineering, November 1999.

[38]Sheldon, D. and Pryor, J., "Study in Depth of a Single Point and Two Point Lateral and Tandem (Longitudinal) Suspensions of Rectangular Box Loads," Technical Report AM/38, The Royal Military College of Science, 1973.

[39]Johnson, E. N. and Schrage, D. P., "System Integration and Operation of a Research Unmanned Aerial Vehicle," *AIAA Journal of Aerospace Computing, Information, and Communication*, Vol. 1, (1), January 2004, pp. 5–18.

[40]De La Torre, G., Johnson, E. N., and Theodorou, E., "Guidance for Slung Load Operations through Differential Dynamic Programming," Proceedings of the 70th American Helicopter Society Annual Forum, May 20–22, 2014.

[41]Talbot, P. D., Tinling, B. E., Decker, W. A., and Chen, R. T., "A Mathematical Model of a Single Main Rotor Helicopter for Piloted Simulation," Technical Report NASA TM-84281, 1982.

[42]Department of Defense, MIL-STD-1797A, *Flying Qualities of Piloted Aircraft*, 1990.

[43]Richardson, J. R., *Quantifying and Scaling Airplane Performance in Turbulence*, Ph.D. thesis, University of Michigan, 2013.